Eur. J. Mineral.
2010, **22**, 595–604
Published online May 2010

$Pb_3Fe^{3+}_2(PO_4)_4(H_2O)$, a new octahedral-tetrahedral framework structure with double-strand chains

STUART J. MILLS[1,2*], UWE KOLITSCH[3,4], RITSURO MIYAWAKI[5], FRÉDÉRIC HATERT[6], GLENN POIRIER[7], ANTHONY R. KAMPF[8], SATOSHI MATSUBARA[5] and EKKEHART TILLMANNS[4]

[1] Department of Earth and Ocean Sciences, University of British Columbia, 6339 Stores Rd, Vancouver, British Columbia, V6T 1Z4, Canada
[2] Geosciences, Museum Victoria, G.P.O. Box 666, Melbourne 3001, Victoria, Australia
*Corresponding author, e-mail: smills@eos.ubc.ca.
[3] Mineralogisch-Petrographische Abt., Naturhistorisches Museum, Burgring 7, 1010 Wien, Austria
[4] Institut für Mineralogie und Kristallographie, Geozentrum, Universität Wien, Althanstraβe 14, 1090 Wien, Austria
[5] Department of Geology, National Museum of Nature and Science, 3-23-1, Hyakunin-cho, Shinjuku, Tokyo 169-0073, Japan
[6] Laboratoire de Minéralogie et de Cristallochimie, B-18, Université de Liège, 4000 Liège, Belgium
[7] Mineral Sciences Division, Canadian Museum of Nature, P.O. Box 3443, Station D, Ottawa, ON K1P 6P4, Canada
[8] Mineral Sciences Department, Natural History Museum of Los Angeles County, 900 Exposition Boulevard, Los Angeles, CA 90007, USA

Abstract: A new lead iron(III) hydrated phosphate, $Pb_3Fe_2(PO_4)_4(H_2O)$, has been synthesised hydrothermally in Teflon-lined stainless steel autoclaves at 220 °C for 7 days, with an initial pH of 1.5. It is the first example of a synthetic hydrous Pb–Fe^{3+} phosphate. Crystals are small, colourless to white prisms, uniaxial (+) and non-pleochroic. The calculated refractive index for white light is $n = 1.95$. Single-crystal structure determination ($R(F) = 0.0457$) shows $Pb_3Fe_2(PO_4)_4(H_2O)$ to be tetragonal, space group $P4_12_12$ (no. 92), with $a = 9.0440(10)$, $c = 16.766(3)$ Å, $V = 1371.4(3)$ Å^3 and $Z = 4$. $Pb_3Fe_2(PO_4)_4(H_2O)$ has a structure type which is based on a tetrahedral–octahedral framework of FeO_6 octahedra sharing corners with PO_4 tetrahedra, with Pb atoms and H_2O molecules occupying voids in the framework. $Pb_3Fe_2(PO_4)_4(H_2O)$ is homeotypic with synthetic $Pb_3Cr_2(PO_4)_4$; both compounds share the same heteropolyhedral topology and the same space group, but only $Pb_3Fe_2(PO_4)_4(H_2O)$ contains an additional position occupied by a water molecule. The octahedral–tetrahedral chain of $Pb_3Fe_2(PO_4)_4(H_2O)$ is topologically similar to double–strand chains found in the structures of hannayite, galliskiite, kapundaite, $PbIn(AsO_4)(AsO_3OH)$ and $Na_{2.88}Fe(PO_4)_2$. Infrared spectroscopy is used to describe the vibrational properties of $Pb_3Fe_2(PO_4)_4(H_2O)$.

Key-words: $Pb_3Fe_2(PO_4)_4(H_2O)$, crystal structure, octahedral–tetrahedral framework, $6s^2$ lone-pair, infrared spectroscopy, kapundaite, galliskiite, hannayite.

1. Introduction

Phosphorus, iron and to a lesser extent lead are common constituents in many environments. In the oxidised zones of Pb–Cu–Zn orebodies, such as those found at Broken Hill in New South Wales, Australia (Birch, 1999), the Tsumeb mine, Namibia (Gebhard, 1999) and the Clara mine in Oberwolfach, Germany (Walenta, 1992), large suites of secondary phosphate minerals occur. Surprisingly, there are only three known Pb–Fe^{3+} phosphate minerals – drugmanite $Pb(Fe,Al)_2(PO_4)_2(OH)_2$ (Van Tassel *et al.*, 1979; King & Sengier-Roberts, 1988; Schnorrer & Schäfer, 1999), kintoreite $PbFe_3(PO_4)_2(OH,H_2O)_6$ (Pring *et al.*, 1995; Kharisun *et al.*, 1997a; Grey *et al.*, 2009) and the recently described pattersonite (Kolitsch *et al.*, 2008), a dimorph of kintoreite. Further three minerals exist which have another element as a major constituent – phosphogartrellite $PbCuFe(PO_4)_2(OH,H_2O)$ (Krause *et al.*, 1998a), brendelite $(Bi,Pb)_2(Fe^{3+},Fe^{2+})O_2(PO_4)(OH)$ (Krause *et al.*, 1998b) and corkite $PbFe_3(PO_4,SO_4)_2(OH,H_2O)_6$ (Lacroix, 1910; Mills, 2007).

Several synthetic anhydrous Pb–Fe^{3+} phosphates have been described in the literature, such as $PbFe_3(PO_4)_3O$ (ICDD–PDF card 54–1184), $PbFe_2(P_2O_7)_2$ (Boutfessi *et al.*, 1996), $Pb_3Fe(PO_4)_3$ (ICDD–PDF card 45–536) and $Pb_3Fe_2(PO_4)_4$ (Malakho *et al.*, 2005), the last one being the anhydrous form of the phase described here. Pb–Fe^{3+} phosphates are generally studied due to their application as glasses

0935-1221/10/0022-2048 $ 4.50
DOI: 10.1127/0935-1221/2010/0022-2048

in the nuclear waste industry (*e.g.*, Reis *et al.*, 2002; Oelkers & Montel, 2008). The family of phosphate glasses, which are based on pyrophosphate groups (P_2O_7), are chemically stable in aqueous solutions and offer an excellent alternative to more conventional glasses such as sodium aluminophosphate glass (*e.g.*, Polyakov *et al.*, 1994) or borosilicate glass (*e.g.*, Deokattey *et al.*, 2003) for the immobilisation of nuclear waste (Karabulut *et al.*, 2000).

As part of an ongoing study into the systematics of natural and synthetic Pb–Fe^{3+} phosphates (Mills, 2007), we report the intriguing and novel crystal structure of $Pb_3Fe_2(PO_4)_4(H_2O)$, which is the first example of a synthetic hydrous Pb–Fe^{3+} phosphate, and also has the potential to be found in nature. We also discuss the close relation to the anhydrous phosphates $Pb_3Cr_2(PO_4)_4$ (Palkina *et al.*, 1977) and $Pb_3Fe_2(PO_4)_4$ (Malakho *et al.*, 2005), the activity of the lone pair of electrons of the Pb^{2+} cations and infrared spectra of the title compound.

2. Synthesis

$Pb_3Fe_2(PO_4)_4(H_2O)$ was synthesised under mild hydrothermal conditions in Teflon-lined stainless steel autoclaves. The crystals were grown using a mixture of the following precursor compounds: reagent grade PbO, $Fe(NO_3)_3(H_2O)_9$, GeO_2 and H_3PO_4 (as an 85 % aqueous solution), with the approximate stoichiometry 1:3:1:1 – the aim being to synthesise Ge-bearing kintoreite, a Pb–Fe^{3+}-phosphate member of the alunite supergroup (general formula $AB_3(XO_4)_2(OH,H_2O)_6$). The Teflon containers were filled with the mechanically blended mixture and were then filled up with distilled water to about 80 % of their inner volume (initial pH: 1.5) and kept at 220 °C (monitored via thermocouples) under autogenous pressure for 7 days. The autoclaves were then slowly cooled from 220 °C to room temperature over 24 h. At the end of the reaction the pH was 1. The reaction products were filtered and washed several times using distilled water. $Pb_3Fe_2(PO_4)_4(H_2O)$ crystallised as colourless to whitish, transparent, striated prismatic crystals up to 0.1 mm in length, and was accompanied by colourless, lustrous crystals of recrystallised GeO_2.

3. Chemical composition and optical properties

Chemical analyses were obtained using a JEOL 733 electron microprobe with Tracor–Northern 5500 and 5600 automation in WDS mode at 15 kV, with beam current of 20 nA and spot size of 2 μm, at the Canadian Museum of Nature, Ottawa. The following standards were used: anglesite (Pb), hematite (Fe) and fluorapatite (P). $Pb_3Fe_2(PO_4)_4(H_2O)$ is unstable in the beam at higher accelerating voltages.

The average of 5 analyses (calculated on the basis of O = 17) gives the empirical formula $Pb_{2.88}Fe^{3+}_{1.90}P_{4.11}H_{1.98}O_{17}$ for the following ranges: PbO 56.8–57.9, Fe_2O_3 13.2–13.9, P_2O_5 25.9–26.1 and H_2O_{calc} 1.59 wt%. The simplified formula is $Pb_3Fe_2(PO_4)_4(H_2O)$, which requires PbO 59.19, Fe_2O_3 14.12, P_2O_5 25.10, H_2O 1.59, total 100.00 wt%. No Ge or any other impurity element was observed in the EMPA analyses.

Optically, $Pb_3Fe_2(PO_4)_4(H_2O)$ crystals are uniaxial (+). The calculated refractive index for white light based on the Gladstone–Dale compatibility (Mandarino, 1981) is $n = 1.95$. The $Pb_3Fe_2(PO_4)_4(H_2O)$ crystals are non-pleochroic.

4. Infrared spectroscopy

The infrared spectrum of $Pb_3Fe_2(PO_4)_4(H_2O)$ (Fig. 1) was recorded with a Nicolet NEXUS spectrometer at the Laboratoire de Minéralogie et de Cristallochimie, Université de Liège, from 32 scans with a 1 cm^{-1} resolution, over the 400–4000 cm^{-1} region. The sample was prepared by intimately mixing 1 mg of sample with KBr in order to obtain a 150 mg homogeneous pellet which was subsequently dried for a few hours at 110 °C. To prevent water contamination, the measurements were performed under a dry air purge.

According to the fundamental vibrational frequencies of the PO_4 tetrahedron (Farmer, 1974), the absorption bands at 1026 and 960 cm^{-1} can be assigned to ν_3, the antisymmetric stretching mode of the PO_4 anion, and the bands at 587, 552 and 519 cm^{-1} can be assigned to ν_4, their bending mode. The band at 880 cm^{-1} probably corresponds to ν_1, the symmetric stretching mode of the distorted PO_4 tetrahedron, but this band is only infrared active when the site symmetry is lowered. Alternatively, the band could be assigned to ν_3, although, considering the distortion noted in the crystal structure (see below), ν_1 is the more likely assignment. In the water/OH regions, one band is observed at 3365 and one at 1546 cm^{-1}, which can be attributed to the water modes. The shift of the band at 1546 cm^{-1} in the water bending region is indicative of a strong hydrogen bond; however, the O...O distance, calculated from the water stretching band at 3365 cm^{-1} using the Libowitzky (1999) curve, gives a distance of about 2.78 Å which is indicative of a medium-strength bond. An apparent very

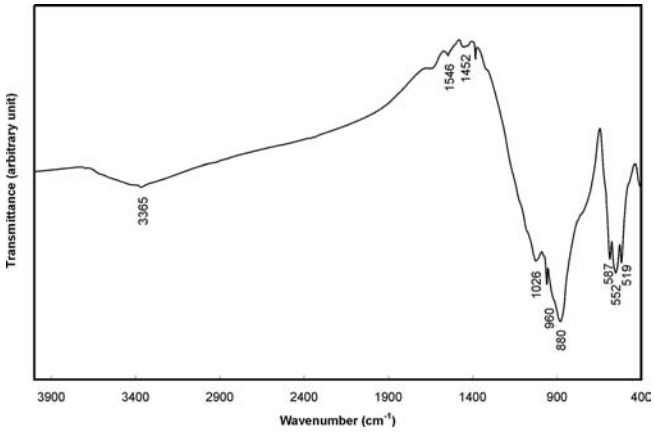

Fig. 1. Infrared spectra for $Pb_3Fe_2(PO_4)_4(H_2O)$.

short hydrogen bond involving a split water position is discussed further below.

5. X-ray diffraction

5.1. X-ray powder diffraction

X-ray powder-diffraction data (Table 1) were collected on a 114.6 mm diameter Gandolfi camera with Ni-filtered Cu$K\alpha$ radiation at the Department of Geology, National Museum of Nature and Science, Japan. The data were recorded on an imaging plate and processed with a Fuji BAS–2500 bio-image analyzer using the computer program written by Nakamuta (1999). Data was calibrated with an internal quartz-standard (reference material NIST SRM #1878a). Unit-cell parameters refined from the powder data using TOPAS (Coelho, 2004) are $a = 9.047(5)$, $c = 16.7840(3)$ Å and $V = 1370.5(4)$ Å^3, which are in good agreement with those obtained from the single-crystal study [$a = 9.0440(10)$, $c = 16.766(3)$ Å and $V = 1371.4(3)$ Å^3].

5.2. Single-crystal structure determination

The single-crystal study was done using a Nonius KappaCCD single-crystal diffractometer equipped with a 300 μm diameter capillary-optics collimator to provide increased resolution. Study of several crystals consistently gave a primitive tetragonal cell, with very good crystal qualities. An optically homogeneous, prismatic crystal with the dimensions 0.08 × 0.05 × 0.02 mm was used for collection of intensity data at 293 K (Table 2). The intensity data were processed with the Nonius program suite DENZO–SMN and corrected for Lorentz, polarisation, and background effects, and, for absorption by the multi-scan method (Otwinowski & Minor, 1997; Otwinowski *et al.*, 2003), for absorption.

The crystal structure of $Pb_3Fe_2(PO_4)_4(H_2O)$ was solved in $P4_12_12$ (no. 92) by direct methods using SHELXS–97 (Sheldrick, 2008) and subsequent Fourier and difference Fourier syntheses, followed by anisotropic full-matrix least-squares refinements on F^2 using SHELXL–97 (Sheldrick, 2008). This led to a final $R_1(F)$ of 0.0457%. For the final refinement steps the model of homeotypic $Pb_3Cr_2(PO_4)_4$ (Palkina *et al.*, 1977) was adopted (see below for comparison of both compounds). The presence of a strong absorber (Pb) precluded the experimental location of H atoms and also led to relatively large maxima in the final difference-Fourier map (Table 2). The presence of ideal racemic twinning is reflected by a refined twin ratio of 0.51(2):0.49. The refined atomic coordinates, site occupancies and displacement parameters are given in Table 3, selected polyhedral bond distances in Table 4, and a bond-valence analysis in Table 5, based on parameters of Brown & Altermatt (1985) and updated parameters for Pb (determined on the OPb_4 encapsulated sphere) put forth by Krivovichev & Brown (2001).

Table 1. Powder X-ray diffraction data for $Pb_3Fe_2(PO_4)_4(H_2O)$.

hkl	d_{calc}	I_{calc}[a]	d_{obs}	I/I_o
001	7.96	4	–	
110	6.395	9	6.398	1
102	6.148	11	6.153	1
111	5.975	43	5.978	37
112	5.085	3	–	
103	4.754	20	4.758	3
021	4.366	5	–	
113	4.208	100	4.199	100
004	4.191	33		
120	4.045	24	4.046	9
022	3.98	3	–	
121	3.932	43	3.934	12
104	3.803	14	3.807	4
122	3.643	16	3.645	4
203	3.515	3	3.513	1
114	3.505	3		
123	3.277	18	3.279	6
220	3.197	42	3.199	16
015	3.144	4	3.144	8
221	3.141	2		
222	2.987	93	2.971	86
115	2.968	82		
031	2.967	11		
124	2.911	29	2.913	15
032	2.837	49	2.838	35
131	2.819	81	2.82	65
223	2.775	2	–	
132	2.707	5	–	
033	2.653	19	2.655	14
215	2.581	30	2.583	20
133	2.546	24	2.545	30
231	2.481	3		
034	2.447	2	–	
232	2.403	2	–	
026	2.377	9	2.379	12
314	2.362	2	–	
017	2.315	4	–	
126	2.299	6	–	
233	2.288	3	–	
040	2.261	9	2.262	14
117	2.242	12	2.243	15
140	2.193	5	2.194	9
315	2.176	16	–	
411	2.175	13	–	
330	2.132	2	–	
331	2.114	3	–	
226	2.104	39	2.1	27
008	2.096	15		
217	2.061	2	–	
036	2.049	9	2.043	14
413	2.042	24		
018	2.042	7		
241	2.008	3	–	
136	1.999	2	1.992	39
333	1.991	11		
044	1.989	24		
242	1.966	2	–	
414	1.943	10	–	
227	1.917	3	1.919	3

[a]Intensities ≥ 2 were calculated using PowderCell (Kraus & Nolze, 1996).

Table 2. Summary of data collection conditions and refinement parameters for $Pb_3Fe_2(PO_4)_4(H_2O)$.

Crystal data	
Cell parameters	$a = 9.0440(10)$ Å $c = 16.766(3)$ Å $V = 1371.4(3)$ Å^3 $Z = 4$
Space group	$P4_12_12$ (no. 92)
Data collection	
Temperature (*K*)	293(2)
λ (Mo*K*α)	0.71073
Crystal shape, size	Prism, 0.08 × 0.05 × 0.02 mm
$2\theta_{max}$ (°)	60.08
Rotation width (°)	1.5
Detector distance (mm)	32
Collection time per degree (s)	200
Reflection range	$-12 \le h \le 12$; $-8 \le k \le 9$; $-23 \le l \le 23$
Total no. reflections	3970
No. unique reflections	1993
No. reflections, $F > 4\sigma(F)$	1895
Absorption coefficient	$\mu = 39.34$ mm^{-1}
R_{merg} on F^2	0.0196
Refinement	
No. parameters	119
R_1, $F > 4\sigma(F)$	0.0457
R_1, all data	0.0488
wR_2 (F^2)[a], all data	0.1087
Flack parameter	0.51(2)
Extinction coefficient	0.0
GOF	1.169
$\Delta\sigma_{min}$, $\Delta\sigma_{max}$ (e/Å^3)	−3.29, 8.29

[a] $w = \frac{1}{\sigma^2(F_o^2)+(0.04P^2+66P)}$, $P = \frac{2F_c^2+\mathrm{Max}(F_o^2,0)}{3}$.

6. Crystal structure and topology

6.1. Structure connectivity and cation coordination

$Pb_3Fe_2(PO_4)_4(H_2O)$ has a framework crystal structure, which contains two Pb, one Fe, two P and nine O atoms in the asymmetric unit (Fig. 2, Table 3). One of the latter oxygens, $O9_w$, is part of a water molecule (see below). No deviation from unit occupancy was observed for any of the atoms (except $O9_w$ and possibly Pb1 and Pb2, see below), confirming that the Ge present in the reaction was not incorporated into the structure of $Pb_3Fe_2(PO_4)_4(H_2O)$.

The connectivity of $Pb_3Fe_2(PO_4)_4(H_2O)$ can be described as a three-dimensional framework of FeO_6 octahedra sharing corners with neighbouring PO_4 tetrahedra (Fig. 2). Specifically, each FeO_6 octahedron shares its six corners with three $P1O_4$ and three $P2O_4$ tetrahedra. The two non-equivalent PO_4 tetrahedra, on the other hand, only share three of their corners with FeO_6 octahedra. The fourth corners (O2 in $P1O_4$ and O3 in $P2O_4$) each act as ligands for one Pb1 and one Pb2 atom. The tetrahedral–octahedral framework connectivity results in relatively large, cylindrical channels (Fig. 3) extending parallel to [110] (diameter *ca*. 2.4 × 2.7 Å, based on the O^{2-} ionic radius of 1.35 Å; Shannon, 1976), and narrow channels

Table 3. Atomic coordinates and displacement parameters (Å^2) for $Pb_3Fe_2(PO_4)_4(H_2O)$.

Atom	*x*	*y*	*z*	U_{eq}/U_{iso}	U_{11}	U_{22}	U_{33}	U_{23}	U_{13}	U_{12}
Pb1	0.13213(6)	0.13213(6)	0.0	0.01348(17)	0.0132(2)	0.0132(2)	0.0140(3)	−0.00283(17)	0.00283(17)	−0.0026(3)
Pb2	0.07837(7)	0.34364(7)	0.26523(3)	0.02156(17)	0.0256(3)	0.0270(3)	0.0121(2)	0.0007(2)	−0.0006(2)	−0.0060(2)
Fe	0.5003(2)	0.25894(18)	0.12075(11)	0.0047(3)	0.0040(8)	0.0066(8)	0.0033(6)	−0.0004(6)	0.0001(6)	−0.0003(7)
P1	0.2283(4)	0.4920(4)	0.07791(18)	0.0069(5)	0.0059(16)	0.0114(17)	0.0034(12)	−0.0007(11)	0.0008(11)	0.0021(11)
P2	0.4681(4)	0.2687(4)	0.31889(19)	0.0074(6)	0.0139(16)	0.0021(14)	0.0063(13)	0.0001(11)	0.0008(11)	−0.0022(11)
O1	0.5226(12)	0.2219(12)	0.2380(6)	0.017(2)	0.021(5)	0.025(6)	0.004(4)	−0.001(4)	0.001(4)	−0.002(4)
O2	0.1025(11)	0.3816(12)	0.0675(6)	0.0143(19)	0.008(5)	0.017(5)	0.018(4)	−0.006(4)	−0.002(4)	−0.004(4)
O3	0.3401(13)	0.3772(12)	0.3149(6)	0.018(2)	0.027(6)	0.012(5)	0.015(4)	0.000(4)	0.004(4)	0.011(4)
O4	0.3589(11)	0.4244(11)	0.1252(5)	0.0102(19)	0.009(4)	0.012(4)	0.009(4)	−0.003(4)	−0.006(4)	0.007(4)
O5	0.0960(11)	0.1684(12)	0.3809(5)	0.0106(18)	0.010(5)	0.014(5)	0.008(4)	0.002(4)	0.002(3)	0.009(4)
O6	0.4234(11)	0.1281(11)	0.3665(5)	0.0074(16)	0.011(4)	0.006(4)	0.005(3)	0.003(3)	0.000(3)	−0.001(4)
O7	0.2169(12)	0.0449(13)	0.2528(6)	0.0157(19)	0.016(5)	0.025(6)	0.006(4)	0.005(4)	0.004(4)	0.001(4)
O8	0.3245(11)	0.1219(11)	0.1190(6)	0.013(2)	0.009(4)	0.010(4)	0.018(5)	0.003(4)	−0.002(4)	−0.007(4)
$O9_w$[a]	−0.150(2)	0.082(2)	0.2375(11)	0.010[b]						

Pb1 and Pb2 are interchanged with respect to those reported by Palkina *et al.* (1977) for $Pb_3Cr_2(PO_4)_4$.
[a]Half-occupied, split position; occupancy fixed to 0.50 (see text).
[b]Fixed.

Table 4. Polyhedral bond distances (Å) in $Pb_3Fe_2(PO_4)_4(H_2O)$.

Pb1–	O2 (×2)	2.538(11)	Pb2–	$O9_w$	2.273(18)	Fe–	O4	1.969(10)	P1–	O7	1.519(10)	P2–	O1	1.504(10)
	O3 (×2)	2.561(11)		O6	2.442(9)		O1	2.004(10)		O2	1.524(9)		O3	1.519(10)
	O8 (×2)	2.648(10)		O5	2.509(9)		O6	2.015(9)		O8	1.549(11)		O5	1.540(10)
	O4 (×2)	2.814(9)		O2	2.526(10)		O8	2.016(10)		O4	1.549(10)		O6	1.555(9)
	av.	2.64		O3	2.527(13)		O5	2.016(9)		av.	1.535		av.	1.530
				O1	2.974(11)		O7	2.030(10)						
				O7	2.986(11)		av.	2.008						
				av.	2.605									

Table 5. Bond-valence analysis for $Pb_3Fe_2(PO_4)_4(H_2O)$.

	Pb1		Pb2	Fe	P1	P2	$\sum$
O1			0.13	0.52		1.36	2.01
O2	0.31	↓×2	0.32		1.29		1.92
O3	0.30	↓×2	0.32			1.30	1.92
O4	0.18	↓×2		0.57	1.20		1.95
O5			0.33	0.50		1.23	2.06
O6			0.38	0.50		1.18	2.06
O7			0.12	0.48	1.30		1.90
O8	0.25	↓×2		0.50	1.20		1.95
$O9_w$			0.53				0.53
$\sum$	2.06		2.12	3.06	4.99	5.07	

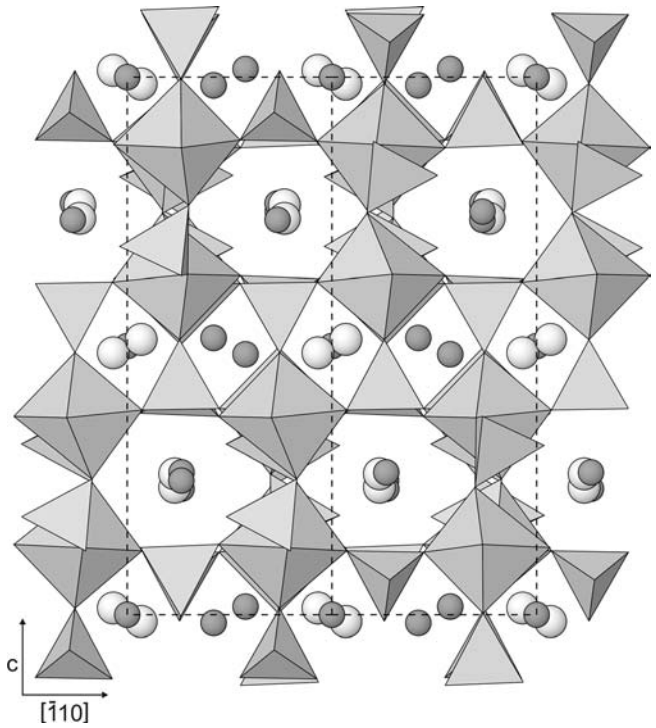

Fig. 2. Crystal structure of $Pb_3Fe_2(PO_4)_4(H_2O)$ projected along [110]. Unit cell outline dashed. Gray spheres are Pb and white spheres are $O9_w$.

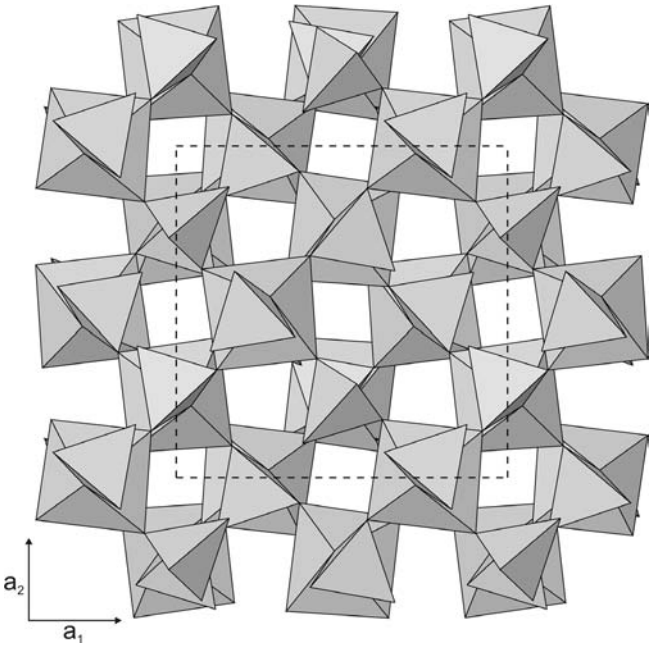

Fig. 3. Crystal structure of $Pb_3Fe_2(PO_4)_4(H_2O)$ projected along [001]. Unit cell outline dashed. Pb and $O9_w$ are not shown.

extending parallel to [101] and [011]. These channels host the two Pb atoms and a half-occupied $O9_w$ site ($O9_w$–$O9_w'$ = 0.97(4) Å). The latter site posed some problems during refinement since unrestrained refinements suggested more than full occupancy (1.16, isotropic treatment; 1.06, anisotropic treatment), whereas for a split $O9_w$ site a refined occupancy of 0.5 would be expected. An alternative model might involve some disorder and partial occupancies involving the Pb atoms substituting to a very minor part for the water molecules on the $O9_w$ site. We point out that we observed in the diffraction patterns very faint streaks (intensity ~2–3 times above background) along c^*. This

feature may be related to some disorder involving the water molecule, the Pb atom and/or other atoms. Tentative refinements of the occupancies of the two Pb sites gave values of 0.940(7) for Pb1 and 0.962(8) for Pb2. Since we were unable to prove this hypothesis, we have restrained the occupancy of the $O9_w$ site to 0.5 to achieve a physically reasonable, albeit simplified model.

A bond-valence analysis (Table 5) showed that the $O9_w$ atom, bonded only to Pb2, belongs to a water molecule (0.53 *v.u.*). The O sites O1 to O8 are all fully occupied by O^{2-} anions as shown by their bond-valence sums between 1.8 and 2.2 *v.u.* and confirm the absence of hydroxyl units in the structure. The quantitative coordination parameters calculated for the Pb, Fe and P sites in $Pb_3Fe_2(PO_4)_4(H_2O)$ are based on the determination of the centroid of coordination (Balić-Žunić & Makovicky, 1996) and the measure of distortion for coordination polyhedra (Makovicky & Balić-Žunić, 1998) and were performed using the program IVTON2 (Balić-Žunić & Vicković, 1996). The inferred O...O hydrogen-bonding distance of about 2.78 Å (derived from the IR spectrum, see above), may reflect the distances from the (split) $O9_w$ atom to O6 (2.85 Å) or O7 (2.87 Å). There appears to be also a further, very short hydrogen bond between $O9_w$ and O5 at 2.56 Å. Such a strong bond will cause a broad bump in the infrared spectrum at roughly around 1000 cm^{-1}. A bump in this region of the IR spectrum (Fig. 1) may in fact be hidden beneath the overlapping PO_4 bands. However, a very strong hydrogen bond $O9_w$...O5 would further increase the already slightly high bond-valence sum of O5 (2.06 *v.u.*, Table 5). For an improved characterisation of the hydrogen-bonding system, polarised single-crystal IR spectroscopic data, possibly in combination with neutron diffraction studies, would be necessary.

The Pb1 atom is located on a four-fold special site (x, x, 0) with point symmetry 2. The atom is in eight-fold coordination, with two sets of shorter bonds, Pb–O2 = 2.538(11) Å and Pb–O3 = 2.561(11) Å, and two sets of longer bonds, Pb–O8 = 2.648(10) Å and Pb–O4 = 2.814(9) Å. The shorter bonds are to oxygen ligands of both the $P1O_4$ and $P2O_4$ tetrahedra, whilst the longer bonds are only to those of the $P1O_4$ tetrahedron. The Pb1–O bonds are slightly longer than those reported for $Pb_3Cr_2(PO_4)_4$ by Palkina *et al*. (1977).

The Pb2 atom sits on an eight-fold general site (x, y, z) with point symmetry 1. The Pb2 atom is in seven-fold coordination, with the seven Pb–O bonds all to different O atoms. The bond distances vary between 2.442(9) Å for Pb–O6 [an O shared between the FeO_6 octahedron (equatorial) and the $P2O_4$ tetrahedron (basal)] and 2.986(11) Å for Pb–O7 [an O shared between the FeO_6 octahedron (basal) and the $P1O_4$ tetrahedron (basal)], with a very short bond to the water molecule, $O9_w$ of 2.273(18) Å. The arrangement of Pb–O bonds indicates that Pb2's lone pair of electrons is stereochemically active (Fig. 4). The Pb1–Pb2 distance in the [110] channels is 3.71 Å. Consideration of the Pb–O bond lengths and grouping of long and short bonds in $Pb_3Cr_2(PO_4)_4$ indicates that the equivalent Pb site in the latter is also stereochemically active.

In the majority of Pb oxysalts, the stereochemical activity of the $6s^2$ Pb^{2+} lone pair of electrons leads to distorted co-ordination, with the Pb–O distances on one side of the ion being longer than the other (*e.g*., joesmithite – Moore, 1988; wherryite – Cooper & Hawthorne, 1994; mawbyite – Kharisun *et al*., 1997b; synthetic $Pb_4BiO_4PO_4$ – Giraud *et al*. 1999) and also to the lowering of symmetry in the crystal structure (*e.g*., hyalotekite – Moore *et al*., 1982; $Sr_{2-x}Pb_x(VO)(VO_4)_2$ solid solution series – Mentre *et al*., 1998). The Pb^{2+} ion on the Pb2 site in $Pb_3Fe_2(PO_4)_4(H_2O)$ shows the first of these two features, with grouping of the short and long O bonds (Fig. 4). This grouping and the volume distortion exhibited in the Pb2–O polyhedron (v = 0.5679) confirms that the $6s^2$ lone-pair is stereochemically active, whilst Pb1 does not have a stereochemically active

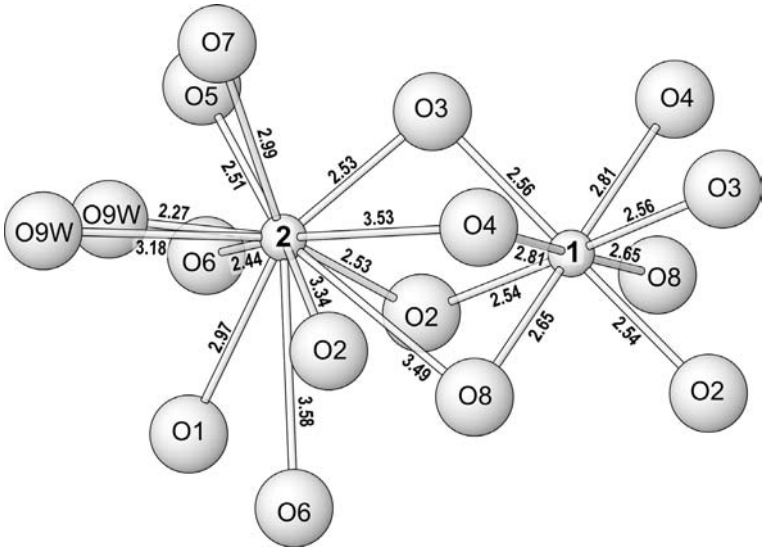

Fig. 4. The coordination spheres for Pb atoms in $Pb_3Fe_2(PO_4)_4(H_2O)$. The lopsided distribution of bond lengths in Pb2 is attributable to the localisation of the lone-pair electrons.

lone-pair. Both Pb atoms are slightly overbonded according to the bond-valence calculations (Table 5), with Pb1 and Pb2 having formal valences of 2.06 and 2.12 *v.u.*, respectively. These values would increase significantly, however, if the older bond-valence parameters of Brown & Altermatt (1985) were used, the increase being most pronounced for Pb2 (due to the stereochemically active lone pair), which would have a formal valence of 2.25 *v.u.* using the older parameters.

The new parameters for Pb were determined on the OPb_4 encapsulated sphere rather than minimising the differences between the formal oxidation state and the experimental bond valence sums (*e.g.*, Mills *et al.*, 2009a). Although OM_4 bonds fit the general r_0–b trend for MO_n (in this case M = Pb), they appear to, on average, overestimate the formal valence of the ion. Since the short bonds to the tetrahedral O will usually all be on the same side of the M atom, away from the lone pair, the resulting unit will link to other parts of the structure through the much longer bonds that make up the rest of the MO_n polyhedron. This feature has recently been described for plumbogummites (Mills *et al.*, 2009b) – Pb–Al-dominant members of the alunite supergroup.

The Fe site in $Pb_3Fe_2(PO_4)_4(H_2O)$ is octahedrally coordinated by O atoms. All the Fe is ferric as shown by the bond-valence calculations (3.06 *v.u.*, Table 5) and as expected from the conditions set by the hydrothermal synthesis. The Fe–O bonds range from 1.969(10) to 2.030(10) Å. The average Fe–O bond length, 2.008 Å, is in good agreement with the grand mean value reported in the literature (*e.g.*, 2.011 Å; Baur, 1981). The FeO_6 octahedron is weakly distorted with a bond-length distortion (BLD) parameter of −0.27 and edge-length distortion (ELD) parameter (Renner & Lehmann, 1986) of −0.12, with the octahedron being stretched in the [110] plane.

The two non-equivalent P atoms in $Pb_3Fe_2(PO_4)_4(H_2O)$ form distorted PO_4 tetrahedra, with the average P–O bond length 1.535 Å for P1 and 1.530 Å for P2; both values are close to the average value observed in phosphates (1.537 Å; Huminicki & Hawthorne, 2002). The two tetrahedra are each characterised by two short and two long P–O bonds (Table 4), reflecting distinct bond-length distortions. The volume distortion parameters for the $P2O_4$ tetrahedron (v = 0.16) indicate that despite <P–O> being close to the ideal value, the shortest bond has resulted in squashing of the tetrahedron. $P1O_4$ on the other hand has a volume distortion parameter of 0.002, indicating almost ideal shape.

6.2. Comparison with related compounds and minerals

Two compounds may be considered as anhydrous formula equivalents of $Pb_3Fe_2(PO_4)_4(H_2O)$: $Pb_3Fe_2(PO_4)_4$ (Malakho *et al.*, 2005) and $Pb_3Cr_2(PO_4)_4$ (Palkina *et al.*, 1977). The first one is monoclinic ($P2_1/c$) and shows no close relation to the structure of the title compound. The second one is tetragonal and crystallises with the same space-group symmetry as $Pb_3Fe_2(PO_4)_4(H_2O)$. In fact, the topologies of both compounds are practically identical, except for the presence of the water molecule ($O9_w$) in the channels of $Pb_3Fe_2(PO_4)_4(H_2O)$ (Fig. 5). Thus, the title compound can be considered homeotypic with $Pb_3Cr_2(PO_4)_4$. The latter compound was prepared by a high-temperature solid-state reaction (Palkina *et al.*, 1977) and is therefore expected to be anhydrous.

The unit-cell parameters given for tetragonal $Pb_3Cr_2(PO_4)_4$ are a = 9.597(3) and c = 16.532(7) Å, but the corresponding entry in the ICSD crystal structure database is accompanied by the comment ''*a,b appear to be 0.7* Å *too long according to given bond lengths*''. The corrected unit-cell parameter would therefore be $a \sim 8.9$ Å, a value which is close to that in the title compound, 9.0440(10) Å. The c parameter in the Cr compound, 16.532(7) Å, is slightly smaller than that in $Pb_3Fe_2(PO_4)_4(H_2O)$ (16.766(3) Å). This may be explained by the ionic radius of $^{[6]}Cr^{3+}$ being smaller than that of $^{[6]}Fe^{3+}$ (0.58 *vs.* 0.69 Å; Shannon, 1976).

Two mineral species have chemical compositions similar to that of the title compound. The first is drugmanite $Pb(Fe,Al)_2(PO_4)_2(OH)_2$ (Van Tassel *et al.*, 1979; King &

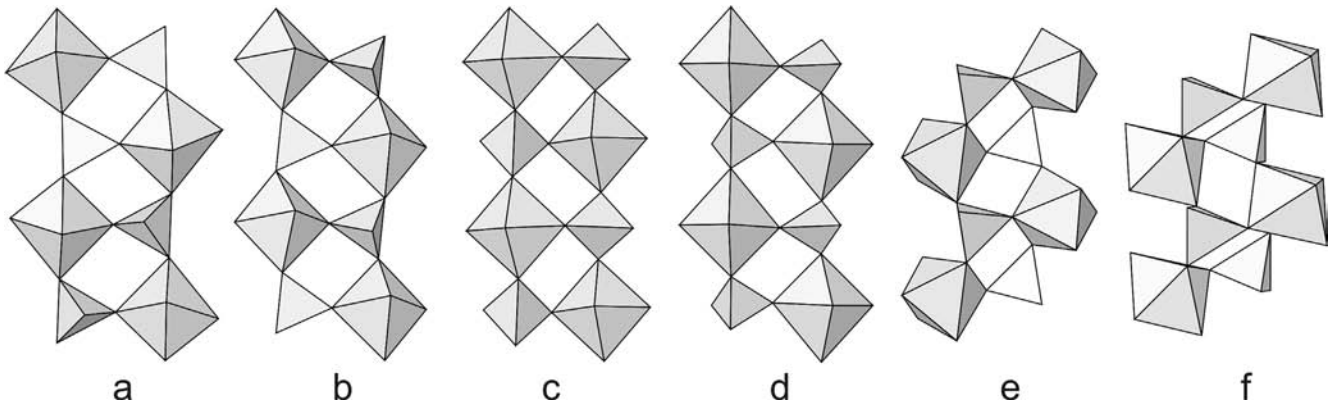

Fig. 5. Octahedral–tetrahedral double–strand chains in (a) $Pb_3Fe_2(PO_4)_4(H_2O)$, (b) hannayite, (c) galliskiite, (d) kapundaite, (e) $Na_{2.88}Fe(PO_4)_2$ and (f) $PbIn(AsO_4)(AsO_3OH)$.

Sengier-Roberts, 1988; Schnorrer & Schäfer, 1999), whose crystal structure is based on kröhnkite-type chains of corner-sharing FeO_6 octahedra and PO_4 tetrahedra (see Kolitsch & Fleck, 2005, and references therein for review on kröhnkite-type minerals and synthetic compounds). The second related mineral is pattersonite, $PbFe_3(PO_4)_2(OH)_4(H_2O_{0.5},OH_{0.5})_2$ (Kolitsch *et al*., 2008) which is also structurally unrelated to the title compound, since pattersonite contains zigzag chains of corner-sharing FeO_6 octahedra which extend in two different directions.

6.3. Octahedral–tetrahedral double-strand chains

The three-dimensional framework of octahedra and tetrahedra in $Pb_3Fe_2(PO_4)_4(H_2O)$ can be viewed as consisting of interpenetrating double-strand chains of octahedra and tetrahedra running parallel to [110] and [$\bar{1}$10]. The chain (Fig. 5a) is topologically similar to double-strand chains found in the structures of hannayite, $Mg_3(NH_4)_2(HPO_4)_4{\cdot}8H_2O$ (Catti & Franchini-Angela, 1976) (Fig. 5b), galliskiite, $Ca_4Al_2(PO_4)_2F_8{\cdot}5H_2O$ (Kampf *et al*., 2010) (Fig. 5c) and kapundaite, $(Na,Ca)_2Fe^{3+}{}_4(PO_4)_4(OH)_3{\cdot}5H_2O$ (Mills *et al*., 2010) (Fig. 5d).

Although the slightly different geometries somewhat obscure the similarities in the chains, the chains in hannayite, galliskiite and kapundaite are topologically equivalent, but differ from that in $Pb_3Fe_2(PO_4)_4(H_2O)$ with respect to the orientation of adjacent tetrahedra. This can best be seen by comparing the chains in hannayite and $Pb_3Fe_2(PO_4)_4(H_2O)$. Along the chains, the unshared tetrahedral vertices in hannayite (Fig. 5b) point alternately up and down, while those in $Pb_3Fe_2(PO_4)_4(H_2O)$ (Fig. 5a) point up–up–down–down.

A similar chain found in $Na_{2.88}Fe(PO_4)_2$ (trisodium iron phosphate) (Fig. 5e), was described as ''hannayite-like'' by Hatert (2007); however, the topologies of these two chains are clearly different. Note that in the $Na_{2.88}Fe(PO_4)_2$ chain the octahedra share three corners of the same octahedral face with tetrahedra, while in all of the other chains the octahedra share three equatorial corners with tetrahedra.

Octahedral–tetrahedral framework structures in which all linkages are via octahedral–tetrahedral corner-sharing appear to be quite rare. Besides $Pb_3Fe_2(PO_4)_4(H_2O)$ [and $Pb_3Cr_2(PO_4)_4$], the only example that we are aware of is that of $PbIn(AsO_4)(AsO_3OH)$ (Kolitsch & Schwendtner, 2005). The octahedra in both structure types share each of their six vertices with tetrahedra and the tetrahedra share three of their four vertices with octahedra. The frameworks are similar in that they both have channels containing Pb in lopsided coordinations due to the lone-pair effect; however, the shapes of the channels differ. The $PbIn(AsO_4)(AsO_3OH)$ framework is also based upon a octahedral–tetrahedral double-strand chain (Fig. 5f), but it runs in only one direction, parallel to the channel. It is also noteworthy that the chain in $PbIn(AsO_4)(AsO_3OH)$ is topologically equivalent to the one in $Na_{2.88}Fe(PO_4)_2$.

Acknowledgements: We thank Editor Roland Oberhänsli, Associate Editor Marco Pasero, and the two referees Werner Krause and Ron Peterson for helpful comments on the manuscript. Prof. Tonči Balić-Žunić (Københavns Universitet) is thanked for providing a copy of IVTON2 and for his insight on distortion of polyhedra. FH acknowledges the Fonds National de la Recherche Scientifique, Belgium, for a position of ''Chargé de Recherches''.

References

Balić-Žunić, T. & Makovicky, E. (1996): Determination of the centroid or ''the best centre'' of a coordination polyhedron. *Acta Crystallogr. B*, **52**, 78–81.

Balić-Žunić, T., & Vicković, I. (1996): IVTON – program for the calculation of geometrical aspects of crystal structures and some crystal chemical applications. *J. Appl. Crystallogr.*, **29**, 305–306.

Baur, W.H. (1981): Interatomic distance predictions for computer simulation of crystal structures. *in* ''Structure and Bonding in Crystals'', M. O'Keeffe, A. Navrotsky, eds., **II**, Academic Press, New York, Chapter 15, 31–52.

—, ed. (1999): The minerals. *in* ''Minerals of Broken Hill'', Broken Hill City Council & Museum of Victoria, Broken Hill, Australia, 88–257.

Boutfessi, A., Boukhari, A., Holt, E.M. (1996): Lead(II) diiron(III) pyrophosphate and barium diiron(III) pyrophosphate. *Acta Crystallogr. C*, **52**, 1594–1597.

Brown, I.D. & Altermatt, D. (1985): Bond-valence parameters obtained from a systematic analysis of the inorganic crystal structure database. *Acta Crystallogr. B*, **41**, 244–247.

Catti, M. & Franchini-Angela, M. (1976): Hydrogen bonding in the crystalline state. Structure of $Mg_3(NH_4)_2(HPO_4)_4(H_2O)_8$ (hannayite), and crystal chemical relationships with schertelite and struvite. *Acta Crystallogr. B*, **32**, 2842–2848.

Coelho, A.A. (2004): *TOPAS*, V3.0, Bruker AXS, Karlsruhe, Germany.

Cooper, M.A. & Hawthorne, F.C. (1994): The crystal structure of wherryite, $Pb_7Cu_2(SO_4)_4(SiO_4)_2(OH)_2$, a mixed sulphate–silicate with $[^{[6]}M(TO_4)_2\Phi]$ chains. *Can. Mineral*., **32**, 373–380.

Deokattey, S., Bhaskar, N., Kalyane, V.L., Kumar, V., Jahagirdar, P.B. (2003): Borosilicate glass and synroc R&D for radioactive waste immobilization: an international perspective. *J. Miner. Met. Mater. Soc*., **55**, 48–51.

Farmer, V.C. (1974): The infrared spectra of minerals. Adlard and Son Ltd., London, 227–331.

Gebhard, G. (1999): Tsumeb II: a Unique Mineral Locality. GG Publishing, Großenseifen, Germany, 328 p.

Giraud, S., Wignacourt, J.-P., Drache, M., Nowogrocki, G., Steinfink, H. (1999): The stereochemical effect of $6s^2$ lone-pair electrons: the crystal structure of a new lead bismuth oxyphosphate $Pb_4BiO_4PO_4$. *J. Solid State Chem*., **142**, 180–188.

Grey, I.E., Mumme, W.G., Mills, S.J., Birch, W.D., Wilson., N.C. (2009): The crystal chemical role of zinc in alunite-type minerals: structure refinements for pure and zincian kintoreite. *Am. Mineral*., **94**, 676–683.

Hatert, F. (2007): Crystal structure of trisodium iron diphosphate, $Na_{2.88}Fe(PO_4)_2$, a synthetic phosphate with hannayite-type heteropolyhedral chains. *Z. Kristallogr.*, **222**, 6–8.

Huminicki, D.M.C. & Hawthorne, F.C. (2002): The crystal chemistry of the phosphate minerals. *Rev. Mineral. Geochem.*, **48**, 123–253.

Kampf, A.R., Colombo, F., Simmons, W.B., Falster, A.U., Nizamoff, J.W. (2010): Galliskiite, $Ca_4Al_2(PO_4)_2F_8{\cdot}8H_2O$, a new mineral from the Gigante granitic pegmatite, Córdoba province, Argentina. *Am. Mineral.*, **95**, 392–396.

Karabulut, M., Marasinghe, G.K., Ray, C.S., Day, D.E., Waddill, G.D., Allen, P.G., Booth, C.H., Bucher, J.J., Caulder, D.L., Shuh, D.K., Grimsditch, M., Saboungi, M.-L. (2000): Local environment of iron and uranium ions in vitrified iron phosphate glasses studied by Fe K and U L_{III}-edge x-ray absorption fine structure spectroscopy. *J. Mater. Res.*, **15**, 1972–1984.

Kharisun, Taylor, M.R., Bevan, D.J.M., Pring, A. (1997a): The crystal structure of kintoreite, $PbFe_3(PO_4)_2(OH,H_2O)_6$. *Mineral. Mag.*, **61**, 123–129.

Kharisun, Taylor, M.R., Bevan, D.J.M., Rae, A.D., Pring, A. (1997b): The crystal structure of mawbyite, $PbFe_2(AsO_4)_2(OH)_2$. *Mineral. Mag.*, **61**, 685–691.

King, G.S.D. & Sengier-Roberts, L. (1988): Drugmanite, $Pb_2(Fe_{0.78}, Al_{0.22})H(PO_4)_2(OH)_2$: its crystal structure and place in the datolite group. *Bull. Minéral.*, **111**, 431–437.

Kolitsch, U. & Fleck, M. (2005): Second update on compounds with kröhnkite-type chains. *Z. Kristallogr.*, **220**, 31–41.

Kolitsch, U. & Schwendtner, K. (2005): Octahedral–tetrahedral framework structures of $InAsO_4{\cdot}H_2O$ and $PbIn(AsO_4)(AsO_3OH)$. *Acta Crystallogr. C*, **61**, i86–i89.

Kolitsch, U., Bernhart, H.-J., Krause, W., Blaβ, G. (2008): Pattersonite, $PbFe_3(PO_4)_2(OH)_4[(H_2O)_{0.5}(OH)_{0.5}]_2$, a new supergene phosphate mineral: description and crystal structure. *Eur. J. Mineral.*, **20**, 281–288.

Krause, W., & Nolze, G. (1996): *POWDER CELL* – a program for the representation and manipulation of crystal structures and calculation of the resulting X-ray powder patterns. *J. Appl. Crystallogr.*, **29**, 301–303.

Krause, W., Belendorff, K., Bernhardt, H.-J. (1998a): Phosphogartrellite, $PbCuFe(PO_4)_2(OH,H_2O)$, a new member of the tsumcorite group. *N. Jb. Mineral. Mh.*, **1998**, 111–118.

Krause, W., Bernhardt, H.-J., McCammon, C., Effenberger, H. (1998b): Brendelite, $(Bi,Pb)_2(Fe^{3+},Fe^{2+})O_2(PO_4)(OH)$, a new mineral from Schneeberg, Germany. *Mineral. Petrol.*, **63**, 263–277.

Krivovichev, S.V. & Brown, I.D. (2001): Are the compressive effects of encapsulation an artifact of the bond valence parameters? *Z. Kristallogr.*, **216**, 245–247.

Lacroix, A.F.A. (1910) As cited in: Anthony, J.W., Bideaux, R.A., Bladh, K.W., Nichols, M.C. (2003): Handbook of Mineralogy, volume V. Borates, Carbonates, Sulfates. Mineral Data Publishing, Tucson, AZ, 813 p.

Libowitzky, E. (1999): Correlation of O–H stretching frequencies and O–H...O hydrogen bond lengths in minerals. *Monatsh. Chem.*, **130**, 1047–1059.

Makovicky, E. & Balić-Žunić, T. (1998): New measure of distortion for coordination polyhedra. *Acta Crystallogr. B*, **54**, 766–773.

Malakho, A.P., Morozov, V.A., Pokholok, K.V., Lazoryak, B.I., Van Tendeloo, G. (2005): Layered ordering of vacancies of lead iron phosphate $Pb_3Fe_2(PO_4)_4$. *Solid State Sci.*, **7**, 397–404.

Mandarino, J.A. (1981): The Gladstone–Dale relationship. IV. The compatibility concept and its application. *Can. Mineral.*, **19**, 441–450.

Mentre, O., Dhaussy, A.-C., Abraham, F., Steinfink, H. (1998): Structural, infrared, and magnetic characterization of the solid solution series $Sr_{2-x}Pb_x(VO)(VO_4)_2$; Evidence of the Pb^{2+} $6s^2$ lone pair stereochemical effect. *J. Solid State Chem.*, **140**, 417–427.

Mills, S.J. (2007): The crystal chemistry and geochronology of minerals from Broken Hill. PhD thesis, University of Melbourne, 249 p.

Mills, S.J., Birch, W.D., Kampf, A.R., Christy, A.G., Pluth, J.J., Pring, A., Raudsepp, M., Chen, Y.-S. (2010): Kapundaite, $(Na,Ca)_2Fe^{3+}{}_4(PO_4)_4(OH)_3{\cdot}5H_2O$, a new phosphate species from Toms quarry, South Australia: description and structural relationship to mélonjosephite. *Am. Mineral.*, **95**, 754–760.

Mills, S.J., Christy, A.G., Chen, E.C.-C., Raudsepp, M. (2009a): Revised values of the bond valence parameters for $^{[4-8]}Sb(V)$–O and $^{[3-11]}Sb(III)$–O. *Z. Kristallogr.*, **224**, 423–431.

Mills, S.J., Kampf, A.R., Raudsepp, M., Christy, A.G. (2009b): The crystal structure of Ga-rich plumbogummite from Tsumeb, Namibia. *Mineral. Mag.*, **73**, 837–845.

Moore, P.B. (1988): The joesmithite enigma: note on the $6s^2$ Pb^{2+} lone pair. *Am. Mineral.*, **73**, 843–844.

Moore, P.B., Araki, T., Ghose, S. (1982): Hyalotekite, a complex lead borosilicate: its crystal structure and the lone-pair effect of Pb(II). *Am. Mineral.*, **67**, 1012–1020.

Nakamuta, Y. (1999): Precise analysis of a very small mineral by an X-ray diffraction method. *J. Mineral. Soc. Japan*, **28**, 117–121. (In Japanese with English abstract).

Oelkers, E.H. & Montel, J.-M. (2008): Phosphate minerals and glasses as potential nuclear waste storage hosts. *Elements*, **4**, 113–116.

Otwinowski, Z. & Minor, W. (1997): Processing of X-ray diffraction data collected in oscillation mode. *in* ''Methods in Enzymology, volume 276: Macromolecular Crystallography A'', C.W. Carter, Jr. & R.M. Sweet, eds., Academic Press, New York, 307–326.

Otwinowski, Z., Borek, D., Majewski, W., Minor, W. (2003): Multiparametric scaling of diffraction intensities. *Acta Crystallogr. A*, **59**, 228–234.

Palkina, K.K., Saifuddinov, V.Z., Lavrov, A.V. (1977): Synthesis and structure of lead(II) chromium(III) phosphate ($Pb_3Cr_2(PO_4)_4$) crystals. *Dokl. Akad. Nauk SSSR*, **237**, 1090–1093 (in Russian).

Polyakov, A.S., Borisov, G.B., Moiseenko, N.I., Osnovin, V.I., Dzekun, E.G., Medvedev, G.M., Bel'tyukov, V.A., Dubkov, S.A., Filippov, S.N. (1994): Experience in operating the ÉP-500/1R ceramic melter for vitrification of liquid high-level wastes. *At. Energy*, **76**, 181–185.

Pring, A., Birch, W.D., Dawe, J.R., Taylor, M.R., Deliens, M., Walenta, K. (1995): Kintoreite, $PbFe_3(PO_4)_2(OH,H_2O)_6$, a new mineral of the jarosite-alunite family, and lusungite discredited. *Mineral. Mag.*, **59**, 143–148.

Reis, S.T., Karabulut, M., Day, D.E. (2002): Structural features and properties of lead–iron–phosphate nuclear wasteforms. *J. Nucl. Mater.*, **304**, 87–95.

Renner, B. & Lehmann, G. (1986): Correlation of angular and bond length distortions in TO_4 units in crystals. *Z. Kristallogr.*, **175**, 43–59.

Schnorrer, G. & Schäfer, H. (1999): Drugmanit, $Pb_2(Fe^{3+},Al)[OH|PO_4]_2.H_2O$, ein drittes Vorkommen aus der Eifel (Grube Neue Hoffnung). *Aufschluss*, **50**, 225–228 (in German).

Shannon, R. (1976): Revised effective ionic radii and systematic studies of interatomic distances in halides and chalcogenides. *Acta Crystallogr. A*, **32**, 751–767.

Sheldrick, G.M. (2008): A short history of *SHELX*. *Acta Crystallogr. A*, **64**, 112–122.

Van Tassel, R., Fransolet, A.-M., Abraham, K. (1979): Drugmanite, $Pb_2(Fe^{3+},Al)(PO_4)_2(OH)\cdot H_2O$, a new mineral from Richelle, Belgium. *Mineral. Mag*., **43**, 463–467.

Walenta, K. (1992): Die Mineralien des Schwarzwaldes. Weise, Munich, Germany, 335 p.

Received 18 January 2010
Modified version received 22 March 2010
Accepted 16 April 2010